Impedance Control Network Resonant dc-dc Converter for Wide-Range High-Efficiency Operation

Impedance Control Network Resonant dc-dc Converter for Wide-Range High-Efficiency Operation

Jie Lu, *Student Member, IEEE,* David J. Perreault, *Fellow, IEEE,* David M. Otten, *Senior Member, IEEE,* and Khurram K. Afridi, *Member, IEEE*

***Abstract*— This paper introduces a new resonant converter architecture that utilizes multiple inverters and a lossless impedance control network (ICN) to maintain zero voltage switching (ZVS) and near zero current switching (ZCS) across wide operating ranges. Hence, the ICN converter is able to operate at fixed frequency and maintain high efficiency across wide ranges in input and output voltages and output power. The ICN converter architecture enables increase in switching frequency (hence reducing size and mass) while achieving very high efficiency. Three prototype 200 W, 500 kHz ICN resonant converters, one with low-Q, one with medium-Q and one with high-Q resonant tanks, designed to operate over an input voltage range of 25 V to 40 V and an output voltage range of 250 V to 400 V are built and tested. The low-Q prototype ICN converter achieves a peak efficiency of 97.1%, maintains greater than 96.4% full power efficiency at 250 V output voltage across the nearly 2:1 input voltage range, and maintains full power efficiency above 95% across its full input and output voltage range. It also maintains efficiency above 94.6% over a 10:1 output power range across its full input and output voltage range owing to the use of burst-mode control.**

***Index Terms*—dc/dc converter, resonant converter, high-efficiency converter, converter for wide-range operation, impedance control network, ZVS and near ZCS; on/off control, burst mode**

I. Introduction

Compact isolated converters operating at large conversion ratios are needed for applications ranging from off-line power supplies for electronic loads to solar micro-inverters. Such converters based on conventional architectures often do not achieve very high efficiencies, and their efficiencies typically drop from peak values as the operating conditions change. To achieve the highest efficiencies, high power density converters must operate using soft-switching techniques – zero voltage switching (ZVS) and/or zero current switching (ZCS) – to limit transistor switching losses. Unfortunately, while conventional soft-switching converter architectures can achieve soft-switching under specific operating conditions, it is difficult to maintain desirable circuit waveforms (e.g., ZVS/ZCS switching and minimum conduction current) as power is reduced from maximum and as the input voltage varies from nominal.

To understand this challenge, consider some widely-used design and control techniques. One common means of controlling resonant soft-switched converters is frequency control, in which the output voltage is regulated in the face of load and input voltage variations by modulating the converter switching frequency [1], [2]. Because of the inductive loading requirements to achieve ZVS switching, power is reduced in such converters by increasing switching frequency, exacerbating switching loss. Wide frequency operation also makes design of magnetic components and EMI filters more challenging. Moreover, depending on resonant tank design, circulating currents in the converter may not back off with power, reducing efficiency. An alternative method is phase-shift control [3], [4] or "outphasing" control, in which the relative timing of multiple inverter legs are modulated to control power. However, conventional full-bridge resonant converters using phase shift control suffer from asymmetric current levels between the two inverter legs at the switching instants as the legs are outphased to reduce output power, as

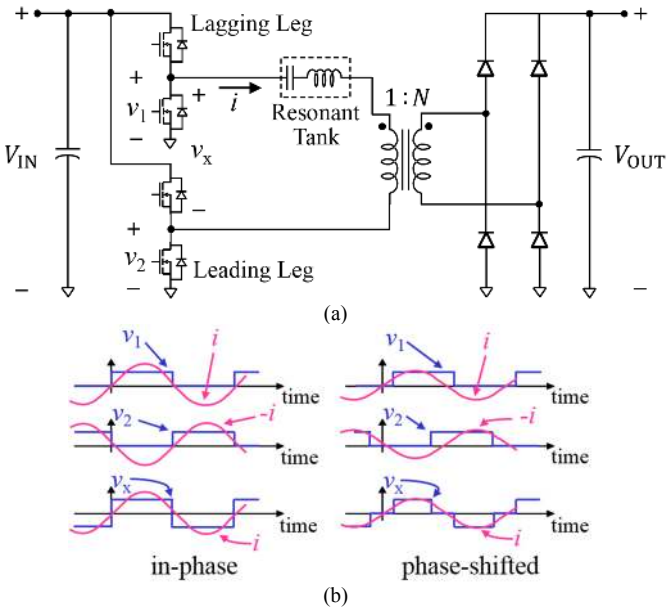

Fig. 1. Asymmetric current levels at switching instants between two inverter legs and eventual loss of ZVS in (a) conventional full-bridge series resonant dc-dc converter as (b) the two inverter legs are phase-shifted to control output voltage or power.

J. Lu and K.K. Afridi are with the Department of Electrical, Computer, and Energy Engineering, University of Colorado Boulder, Boulder, CO 80309 USA (email: jie.lu@colorado.edu; khurram.afridi@colorado.edu).

D.J. Perreault and D.M. Otten are with the Department of Electrical Engineering and Computer Science, Massachusetts Institute of Technology, Cambridge, MA 02139 USA (e-mail: djperrea@mit.edu; otten@mit.edu).

shown in Fig. 1. The result is that the transistors in the leading inverter leg start to turn off at large currents. Also, as outphasing is increased further, the transistors in the lagging inverter leg lose ZVS turn-on capability. These factors result in extra losses and lead to lower converter efficiency at partial loads, and consequently to poor design tradeoffs. Other fixed frequency control techniques have also been developed [5], [6]. However, these also lose zero voltage switching (ZVS) capability as the output power is reduced [7]. Hence, there is need for circuit designs and associated controls that can provide reduced loss when operating over wide input voltage and power ranges, and can provide large voltage conversion ratios.

This paper introduces a new resonant converter architecture that operates at fixed frequency and utilizes a lossless impedance control network (ICN) to maintain ZVS and near-ZCS across wide operating ranges in terms of input/output voltages and output power, minimizing device stress and switching loss, and enabling both high efficiency and power density. Three prototype 200 W, 500 kHz ICN resonant converters, one with low-Q, one with medium-Q and one with high-Q resonant tanks, designed to operate over an input voltage range of 25 V to 40 V and an output voltage range of 250 V to 400 V are built and tested. The low-Q prototype ICN converter achieves a peak efficiency of 97.1%, maintains greater than 96.4% full power efficiency at 250 V output voltage across the nearly 2:1 input voltage range, and maintains full power efficiency above 95% across its full input and output voltage range. It also maintains efficiency above 94.6% over a 10:1 output power range across its full input and output voltage range owing to the use of burst-mode control. This work represents an expansion on an earlier paper [20], and includes additional experimental results and analysis.

The remainder of this paper is organized as follows: Section II describes the architecture, topology and control of the proposed ICN dc-dc converter. Section III describes a methodology for the design of an ICN converter. The design and implementation of the three prototype ICN converters is also described in this section. The experimental results from the three prototypes are presented in section IV. Finally, the conclusions of the paper are summarized in section V.

II. Impedance Control Network (ICN) Resonant Converter

Resonant dc-dc converters comprise an inverter stage, a transformation stage, and a rectifier stage, as shown in Fig. 2. Figure 3 shows the architecture of the proposed impedance control network (ICN) resonant dc-dc converter. It incorporates multiple inverters and one or more rectifiers operated together under phase-shift control, along with a transformation stage incorporating an impedance control network (ICN). The ICN draws upon the concepts of lossless power combiners and resistance compression networks [8]-[16]. The ICN provides a differential phase shift in the voltages and currents whereby the effective impedances seen at its inputs look highly resistive at the fundamental frequency, enabling switching of the inverters

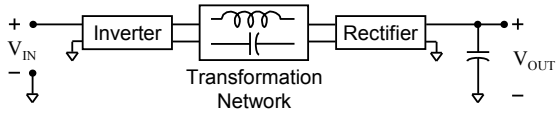

Fig. 2. Block diagram for a conventional dc-dc resonant converter.

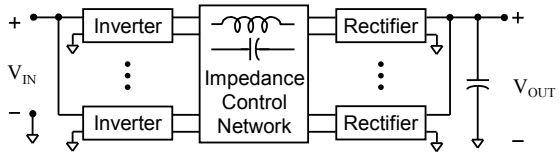

Fig. 3. Architecture of the proposed impedance control network (ICN) resonant converter. Note that while an input parallel connection of inverter inputs is shown, a series connection may also be employed, and can be advantageous for voltage step-down designs.

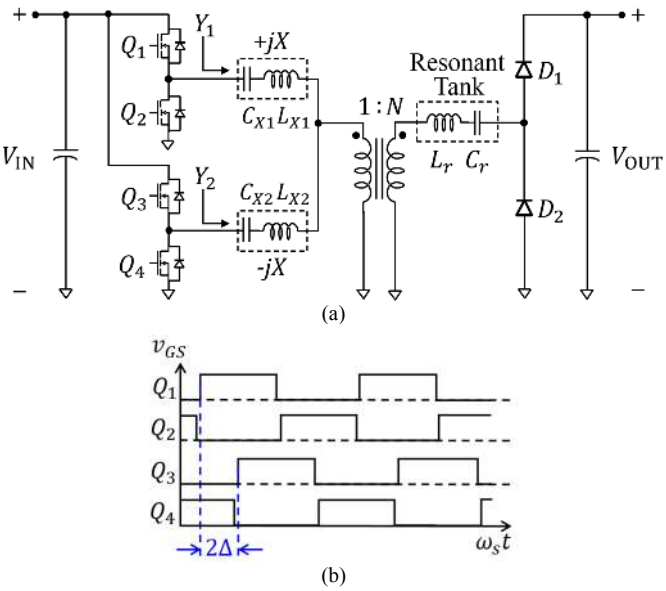

Fig. 4. One implementation of an impedance control network (ICN) resonant converter, appropriate for voltage step-up: (a) converter topology and (b) switch gating signals.

at zero current across wide operating ranges[1]. By modifying the networks for slightly inductive loading of the inverters, one can realize simultaneous zero-voltage and near-zero-current switching.

There are many possible implementations of the ICN converter. A specific implementation suitable for widely varying input voltages is shown in Fig. 4. The converter is operated at a fixed switching frequency and each inverter is operated at a fixed duty ratio (~50%). When the switching frequency of the converter matches the resonant frequency of the resonant tank, and the two branches of the impedance control network are designed to have equal but opposite reactances ($+jX$ and $-jX$) at the switching frequency, the effective admittances seen by the two inverters (Y_1 and Y_2 of Fig. 4) under fundamental frequency approximation and

[1] Here "effective impedance" means the voltage-to-current (V/I) ratio observed at a port with all sources and loads active.

assuming a lossless converter are given by:

$$Y_1 = Y_2^* = \frac{V_{OUT}\sin\Delta}{NV_{IN}X} + j\left(\frac{V_{OUT}\cos\Delta}{NV_{IN}X} - \frac{1}{X}\right). \quad (1)$$

Here V_{IN} is the input voltage, V_{OUT} is the output voltage, N is the transformer turns ratio, and 2Δ is the phase shift between the two inverters. The derivation of (1) is provided in Appendix A. With the two branches of the impedance control network designed to have differential reactances, the effective susceptance seen by the two inverters can be made zero or arbitrarily small when the two inverters are operated with a specific phase shift between them, as illustrated in Fig. 5. The phase shift at which the susceptance seen by the inverters becomes zero is a function of the input-output voltage ratio and given by:

$$2\Delta = 2\cos^{-1}\left(\frac{NV_{IN}}{V_{OUT}}\right). \quad (2)$$

Hence, by varying this phase shift as the input or output voltage varies, the admittance seen by the inverters can be kept purely conductive across the full input and output voltage operating range of the dc-dc converter. By operating the converter at a switching frequency slightly higher than the resonant frequency of the L_r-C_r tank, both the inverters can be slightly inductively loaded to achieve ZVS. This allows the inverter switches to have simultaneous zero-voltage switching and near zero-current switching capability, thus minimizing switching losses and reactive currents, boosting converter efficiency over wide input and output voltage ranges.

At a given switching frequency, the output power of an inverter is proportional to the square of the input voltage and the conductance seen by the inverter. In conventional designs, this can often lead to large variations in power delivery with input voltage that must be addressed (e.g., through oversizing of the inverter components and use of frequency control to modulate power). However, since the effective conductance seen by the inverters in the ICN converter (operated at near zero effective susceptance) decreases with input voltage (see Fig. 5 and Fig. 6), the variation in output power with input voltage can be made quite limited across a wide input voltage range, as shown in Fig. 7, and expressed mathematically as:

$$P_{OUT} = \frac{4V_{IN}\sqrt{V_{OUT}^2 - N^2V_{IN}^2}}{\pi^2 NX}. \quad (3)$$

This expression is derived assuming a lossless converter and utilizing (1) and (2), i.e., under fundamental frequency approximation. Appendix A provides the derivation of (3). The limited variation in output power with input voltage enables improved sizing of inverter components and use of fixed-frequency operation, with consequent benefits for efficiency. Output power of the converter can be further controlled (for values below that indicated in Fig. 7) using burst mode (on/off) control, in which the operation of the converter is modulated on and off at a frequency much lower than its switching frequency [17]-[19]. On/off control is desirable because converter losses back off proportionally to power delivered, thus enabling efficient operation to be maintained over a wide power range.

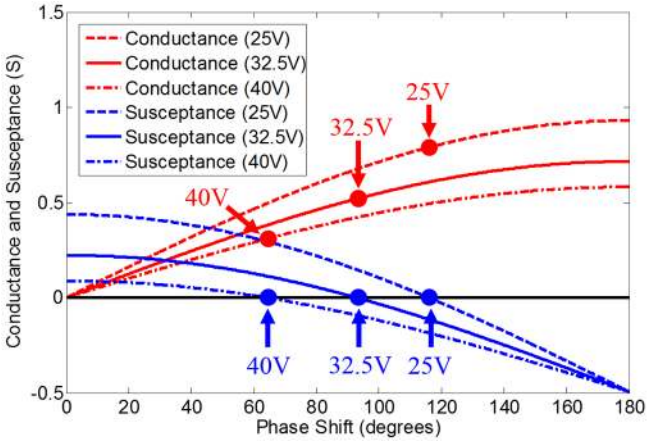

Fig. 5. Effective conductance (real part of Y_1 or Y_2 as given by (1)) and susceptance (absolute value of imaginary part of Y_1 or Y_2) seen by the two inverters as a function of their relative phase shift for three input voltage values: 25 V, 32.5 V and 40 V. In all cases, output voltage is 250 V, X is 2.026 Ω and N is 5.3.

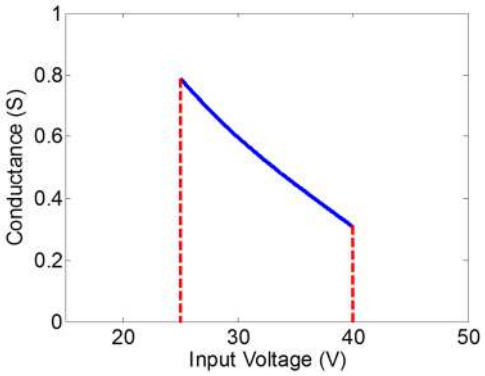

Fig. 6. Effective conductance seen by the two inverters (real part of Y_1 or Y_2, as given by (1)) as a function of input voltage when the ICN converter with X equal to 2.026 Ω and N equal to 5.3 is operated with zero effective susceptance, at output voltage of 250 V.

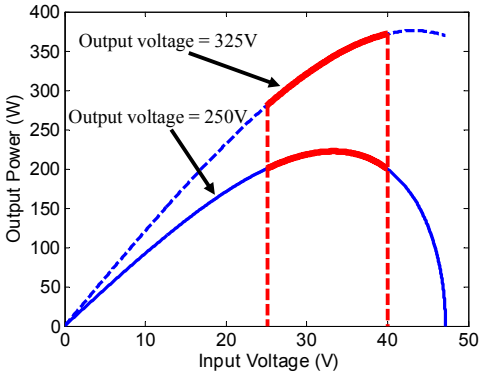

Fig. 7. Variation in output power as a function of input voltage for the ICN converter operated with the phase-shift between the two inverters controlled to provide zero effective susceptance seen by the inverters. The values of X and N in this ICN converter are 2.026 Ω and 5.3, respectively.

Thus, with the proposed architecture we are able to achieve wide voltage and power range operation at fixed switching frequency and high efficiency.

It is instructive to consider the similarities and differences

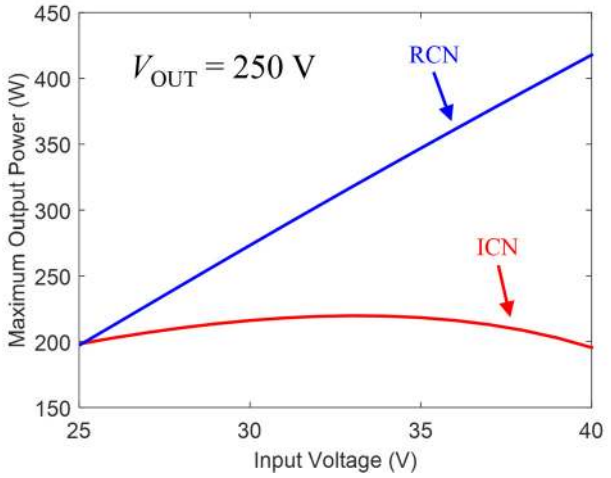

(a)

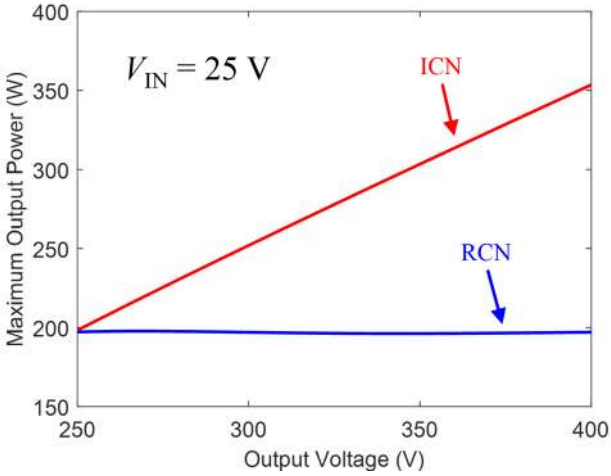

(b)

Fig. 8. Maximum output power delivered by the ICN converter and the RCN converter against (a) an input voltage range from 25 V to 40 V, and (b) an output voltage range from 250 V to 400 V. The switching frequency used in both cases is 500 kHz.

between the ICN converter and a resistance compression network (RCN) converter [13]. They both use burst mode control to regulate output voltage and power, and both can maintain ZVS and near ZCS across a wide range of input voltage, output voltage and power levels. However, while RCN converter utilizes a power splitting network in the rectification stage, the ICN converter uses a power combining network in the inversion stage. The power splitting network of the RCN converter compresses the change in impedance seen by its inverter even though the effective rectifier resistance changes due to variations in input voltage and output power. In a sense, while the RCN converter offers passive compression of its impedance seen by its inverters, the ICN converter offers active control of the impedances of its inverters. A major practical difference between the ICN and RCN-based approaches is in terms of the variations in their maximum output power characteristics with respect to input and output voltages. The maximum output power of the RCN converter is highly invariant to output voltage, while the maximum output power of the ICN converter is highly invariant to input voltage, as can be seen in Fig. 8. Figure 8(a) compares the maximum output power delivered by the ICN converter and a RCN converter designed to meet the same specifications as a function of input voltage. The variation in the maximum output power of the ICN converter is quite limited across the entire input voltage range, while that of the RCN converter increases linearly with input voltage. At the maximum input voltage, the maximum output power of the RCN converter is over twice that of the ICN converter. Figure 8(b) compares the maximum output power delivered by the two converters as a function of output voltage. Now the maximum output power delivered by the RCN converter is nearly constant, while the maximum output power of the ICN converter increases monotonically with output voltage. At the maximum output voltage, the ICN converter delivers maximum output power that is 1.75 times larger than that of the RCN converter. Thus, the ICN converter is more suitable for applications having large variations in input voltages, while the RCN converter is more suitable for applications where the output voltage has large variations.

III. Prototype Design

The ICN resonant converter shown in Fig. 4 has been designed and built with specifications suitable for an interface between a solar photovoltaic (PV) module and a dc distribution system: an input voltage range of 25 V to 40 V, an output voltage range of 250 V to 400 V, and a maximum output power of 200 W. The converter is designed for a switching frequency of 500 kHz.

A. Design Methodology

The maximum output power of the ICN converter increases with output voltage (see Fig. 7); therefore, if maximum output power can be delivered at minimum output voltage then maximum output power can be delivered at all output voltages. Also given the variation in output power with input voltage (see Fig. 7), the need for burst mode control can be minimized if the converter is designed to deliver the same output power at its minimum and maximum input voltages. This requirement can be met at the minimum output voltage if the transformer turns ratio N and the reactance X of the impedance control network are selected using:

$$N = \frac{V_{\mathrm{OUT,min}}}{\sqrt{V_{\mathrm{IN,min}}^2 + V_{\mathrm{IN,max}}^2}}, \tag{4}$$

$$X = \frac{4V_{\mathrm{IN,min}}\sqrt{V_{\mathrm{OUT,min}}^2 - N^2 V_{\mathrm{IN,min}}^2}}{\pi^2 N P_{\mathrm{OUT,max}}}, \tag{5}$$

where $V_{\mathrm{IN,min}}$ is the minimum input voltage, $V_{\mathrm{IN,max}}$ is the maximum input voltage, $V_{\mathrm{OUT,min}}$ is the minimum output voltage and $P_{\mathrm{OUT,max}}$ is the maximum output power. For the given design specifications, N is 5.3 and X is 2.03 Ω.

Once the required differential reactance X is known, the next step is to come up with the design equations for the individual reactive component values. As can be seen from Fig. 4, there are three series resonant tanks in the impedance control network. These tanks serve two purposes: i) provide the

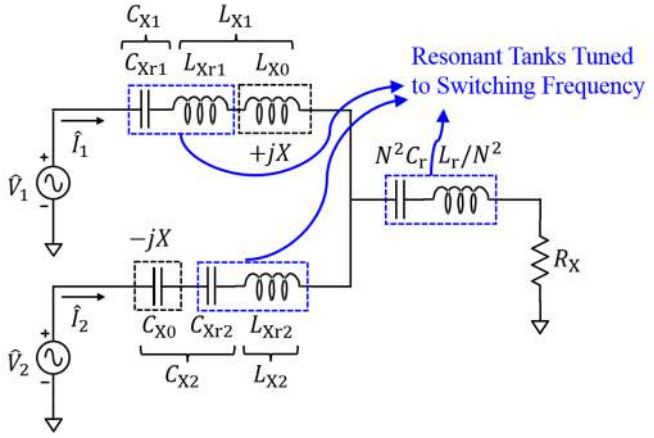

Fig. 9. Primary side reactive elements broken up into their conceptual constituents: differential reactances L_{X0} and C_{X0}, and series resonant tank elements (L_{Xr1}, C_{Xr1}, L_{Xr2} and C_{Xr2}). In the top branch, L_{X0} and L_{Xr1} collectively form L_{X1} and C_{Xr1} is simply C_{X1} of Fig. 4. In the bottom branch, C_{X0} and C_{Xr2} collectively form C_{X2} and L_{Xr2} is simply L_{X2} of Fig. 4. The $\hat{V}_1$ and $\hat{V}_2$ are the fundamental components of the output voltages of the inverters, and the $\hat{I}_1$ and $\hat{I}_2$ are the fundamental components of the output currents of the inverters.

necessary differential reactances; and ii) filter higher-order harmonics. More specifically, the L_{X1}-C_{X1} tank provides the $+jX$ reactance and some filtering of the harmonics, the L_{X2}-C_{X2} tank provides the $-jX$ reactance and also some filtering, and the L_r-C_r tank only provides filtering of higher-order harmonics. Hence, part of the L_{X1}-C_{X1} tank needs to be tuned to the switching frequency to filter out higher-order harmonics, and the remaining part needs to provide the $+jX$ reactance. Likewise, one part of the L_{X2}-C_{X2} tank needs to be tuned to the switching frequency for filtering, and the remaining part needs to provide the $-jX$ reactance. Hence, to determine the values of these reactive components it is simplest to split L_{X1} into two series inductors L_{X0} and L_{Xr1}; and split C_{X2} into two series capacitors C_{X0} and C_{Xr2}. With this division, L_{X0} of the top tank can provide the $+jX$ reactance, and L_{Xr1} together with C_{X1} form the filter. For the bottom tank, C_{X0} can provide the $-jX$ reactance, and L_{X2}-C_{Xr2} form the filter. Figure 9 shows the model of the ICN converter under fundamental frequency approximation. The division of the two tanks (L_{X1}-C_{X1} and L_{X2}-C_{X2}) is also shown in Fig. 9. Also C_{X1} is relabelled as C_{Xr1} and L_{X2} is relabelled as L_{Xr2}. The voltage source $\hat{V}_1$ models the fundamental component of the output voltage of the top inverter, the voltage source $\hat{V}_2$ models the fundamental component of the output voltage of the bottom inverter, and the phase difference between $\hat{V}_1$ and $\hat{V}_2$ has the specific value determined by (2) to make the susceptance seen by the inverters zero. The remaining parts of the ICN converter of Fig. 4 are the transformer, the L_r-C_r tank, the rectifier and the load. Under fundamental frequency approximation a rectifier can be modeled as a resistor (see [2], [10] for equivalent modeling of rectifiers). In Fig. 9 the resistor that models the rectifier and the L_r-C_r tank have been reflected to the primary side of the transformer.

The values of the differential reactive elements (L_{X0} and C_{X0}) are determined using:

$$L_{X0} = \frac{X}{\omega_s}, \tag{6}$$

$$C_{X0} = \frac{1}{X\omega_s}, \tag{7}$$

where ω_s is the angular switching frequency of the converter. The values of the resonant tank elements are determined using:

$$L_{Xr1} = \frac{Z_{0X1}}{\omega_s},\ L_{Xr2} = \frac{Z_{0X2}}{\omega_s},\ L_r = N^2\frac{Z_{0r}}{\omega_s}, \tag{8}$$

$$C_{Xr1} = \frac{1}{Z_{0X1}\omega_s},\ C_{Xr2} = \frac{1}{Z_{0X2}\omega_s},\ C_r = \frac{1}{N^2 Z_{0r}\omega_s}, \tag{9}$$

where Z_{0X1}, Z_{0X2} and Z_{0r} are the desired characteristic impedances of the tanks ($\equiv\sqrt{L_{Xr1}/C_{Xr1}}$, $\sqrt{L_{Xr2}/C_{Xr2}}$, and $\sqrt{L_r/C_r}/N^2$, respectively). Their values are determined from $Z_{0X1} = Q_{0X1}R_X$, $Z_{0X2} = Q_{0X2}R_X$ and $Z_{0r} = Q_{0r}R_X$, where Q_{0X1}, Q_{0X2}, and Q_{0r} are the desired loaded quality factors of the resonant tanks, and R_X ($=2V_{OUT}^2/\pi^2N^2P_{OUT}$) is the equivalent resistance of the rectifier referred to the primary side of the transformer.

B. Selection of Resonant Tank Quality Factors (Q)

The selection of the quality factors of the resonant tanks is a major design consideration in the ICN converter as they impact the level of filtering of the higher order harmonics and value of the resonant inductance. If the resonant tanks are designed to have relatively high quality factors (high-Q) then the tank currents will be almost perfectly sinusoidal but the values of the resonant inductances will be high (with commensurately large inductor size and series resistance). On the other hand, low quality factor (low-Q) designs will require small resonant inductance values leading to reduced losses in the inductor. However, in the low-Q designs the tank currents will not be perfectly sinusoidal. The relatively non-sinusoidal tank currents in the low-Q design could increase turn-off switching losses. To explore the tradeoffs between the above-mentioned conduction and switching losses, a series of ICN converters have been designed with different quality factors for the resonant tanks.

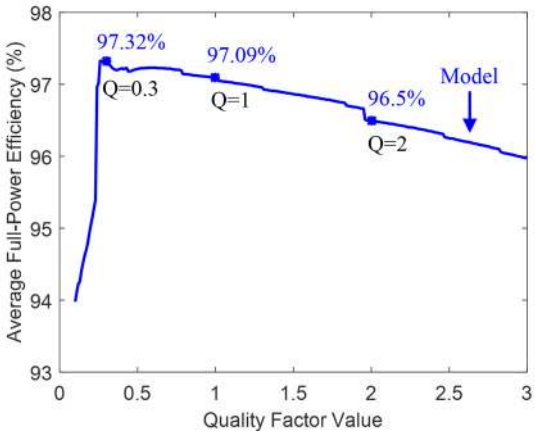

Fig. 10. Theoretically predicted average full-power efficiencies of ICN converters versus the Q value of their resonant tanks. In all converters, the switching frequency is 505 kHz.

The tank Q for the different designs is varied from 0.1 to 3 in step size of 0.01. For each design, the full-power efficiencies are calculated (using an accurate loss model introduced in Appendix B) and averaged over four corner operating points: 25 V input voltage and 250 V output voltage; 25 V input voltage and 400 V output voltage; 40 V input voltage and 250 V output voltage; and 40 V input voltage and 400 V output voltage. The resultant average full-power efficiencies for these ICN converters are plotted against their Q in Fig. 10. As can be seen from Fig. 10, the average efficiency reaches a peak value of 97.32% when Q is around 0.3. The average efficiency decreases slowly above this value of Q, and drops sharply below it. To verify these theoretical results, three ICN converters with resonant tank Q values of 0.3 (low-Q), 1 (medium-Q) and 2 (high-Q) are built and tested.

C. Component Values

For the low-Q ICN converter, the quality factors of the resonant tanks are approximately 0.3 (Q_{0X1} = 0.28, Q_{0X2} = 0.29, and Q_{0r} = 0.41) when R_X has its minimum value of 2.25 Ω (corresponding to the operating point V_{OUT} = 250 V and P_{OUT} = 200 W). For the given specifications, the values of the reactive components are: $L_{X1} = L_{X0} + L_{Xr1}$ = 0.645 μH + 0.2 μH = 0.845 μH, $C_{X1} = C_{Xr1}$ = 507 nF, $L_{X2} = L_{Xr2}$ = 0.211 μH, and $C_{X2} = C_{Xr2} \parallel C_{X0}$ = 480 nF ∥ 157.1 nF = 118 nF, L_r = 8.34 μH and C_r = 10 nF. For the medium-Q ICN converter, the actual quality factors are: Q_{0X1} = 0.96, Q_{0X2} = 1.13, and Q_{0r} = 1. For the given specifications, the values of the tank elements are $L_{X1} = L_{X0} + L_{Xr1}$ = 0.645 μH + 0.685 μH = 1.33 μH, $C_{X1} = C_{Xr1}$ = 147 nF, $L_{X2} = L_{Xr2}$ = 0.81 μH, and $C_{X2} = C_{Xr2} \parallel C_{X0}$ = 125 nF ∥ 157.1 nF = 69.6 nF, L_r = 19.1 μH and C_r = 4.9 nF. For the high-Q ICN converter, the actual quality factors are: Q_{0X1} = 2, Q_{0X2} = 2, and Q_{0r} = 2. For the given specifications, the values of the tank elements are $L_{X1} = L_{X0} + L_{Xr1}$ = 0.645 μH + 1.44 μH = 2.085 μH, $C_{X1} = C_{Xr1}$ = 70.6 nF, $L_{X2} = L_{Xr2}$ = 1.44 μH, $C_{X2} = C_{Xr2} \parallel C_{X0}$ = 70.6 nF ∥ 157.1 nF = 48.71 nF, L_r = 38.5 μH, and C_r = 2.4 nF. The above component values are determined under fundamental frequency approximation, which neglects the effect of higher order harmonics. In practice, due to the presence of higher order harmonics, with these component values the currents through the two branches of the ICN converter are not balanced. To balance these currents the value of C_r is slightly altered from its designed value (see Table I). Considering that the actual component values in a practical design may vary from their desired values, the robustness of the ICN converter's performance to these variations is investigated and discussed in Appendix C.

The actual components used in the fabrication of the three prototype ICN resonant converters are listed in Table I. The core material chosen for the magnetic elements (inductors and transformer) for all three converters is N49 from EPCOS since it has low losses around 500 kHz. Litz wire is used to wind the inductors and the transformer. The primary side resonant capacitors are 250-V NP0 low-ESR capacitors, while 1-kV mica low-ESR capacitors are used for the secondary side resonant capacitors. For the half-bridge inverters, EPC 100-V/25-A enhancement-mode gallium nitride (GaN) transistors (EPC2001) are used. These are driven by half-bridge drivers designed for enhancement-mode GaN transistors (LM5113). For the rectifier stage 600-V/2-A silicon carbide (SiC) Schottky

TABLE I

ACTUAL COMPONENTS USED IN THE PROTOTYPE ICN RESONANT CONVERTERS

Component	Low-Q Design	Medium-Q Design	High-Q Design
Q_1, Q_2, Q_3, Q_4	EPC2001, 100-V/25-A eGaN FETs		
D_1, D_2	C3D02060E, 600-V/2-A Schottky Diodes		
L_{X1}	0.89 μH Core: RM10 EPCOS N49 Winding: 4 turns of 4000-strands 48 AWG litz wire	1.38 μH Core: RM12 EPCOS N49 Winding: 4 turns of 6000-strands 48 AWG litz wire	2.147 μH Core: RM12 EPCOS N49 Winding: 5 turns of 6000-strands 48 AWG litz wire
C_{X1}	507 nF 250-V NP0	141 nF 250-V NP0	68 nF 250-V NP0
L_{X2}	0.25 μH Core: RM10 EPCOS N49 Winding: 2 turns of 4000-strands 48 AWG litz wire	0.84 μH Core: RM10 EPCOS N49 Winding: 3 turns of 4000-strands 48 AWG litz wire	1.508 μH Core: RM10 EPCOS N49 Winding: 4 turns of 4000-strands 48 AWG litz wire
C_{X2}	115 nF 250-V NP0	68 nF 250-V NP0	47 nF 250-V NP0
L_r	8.11 μH Core: RM12 EPCOS N49 Winding: 10 turns of 450-strands 46 AWG litz wire	18.8 μH Core: RM10 EPCOS N49 Winding: 19 turns of 450-strands 46 AWG litz wire	39 μH Core: RM10 EPCOS N49 Winding: 27 turns of 450-strands 46 AWG litz wire
C_r	8.72 nF 1000-V Mica	4.66 nF 1000-V Mica	2.47 nF 1000-V Mica
T_X	1 : 5.33, RM10 EPCOS N49 core, Primary winding: 3 turns of 2000-strands 48 AWG Litz wire, Secondary winding: 16 turns of 450-strands 46 AWG Litz wire, Leakage inductance referred to the secondary side: 2.16 μH		
C_{IN}	2.2 mF × 2, 63-V electrolytic capacitors		
C_{OUT}	47 μF × 1, 450-V electrolytic capacitors		

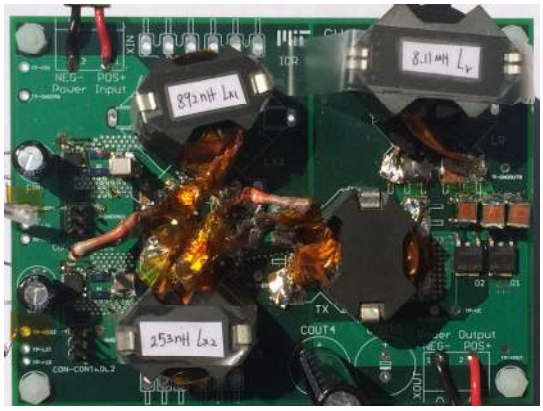

(a)

(b)

Fig. 11. Photograph of the (a) top and (b) bottom of the prototype low-Q ICN resonant converter.

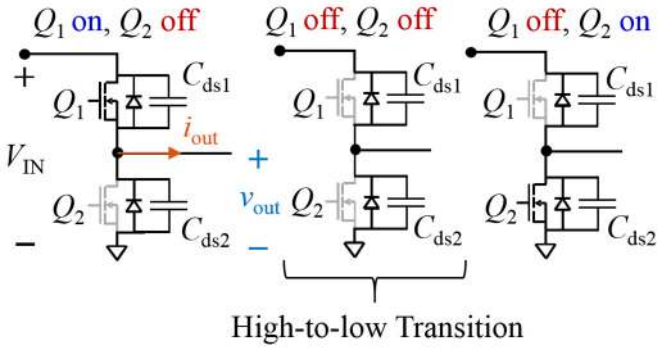

(a)

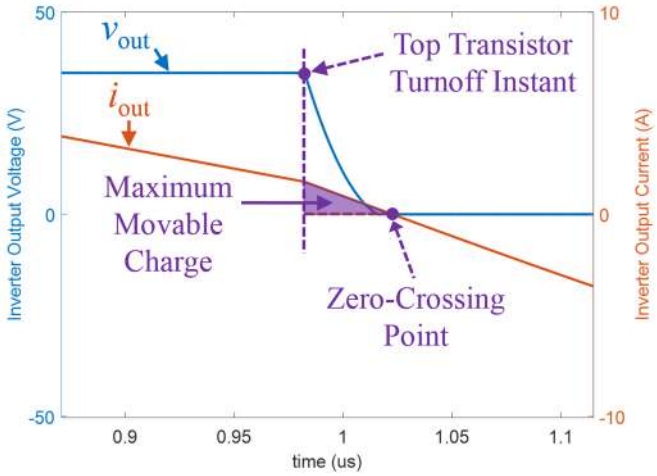

(b)

Fig. 12. High-to-low transition of a half bridge inverter: (a) switch states during the transition, and (b) inverter output voltage and output current waveforms and definition of maximum movable charge.

diodes (C3D02060E) are used. The converter is controlled using a Microchip dsPIC33FJ64GS610, a 16-bit digital signal controller with high-speed PWM outputs. Figure 11 shows the top and bottom views of the prototype low-Q ICN resonant converter.

Since the ICN converters are operated in relatively low frequency burst mode to regulate output voltage and power, substantial input and output capacitance is needed to limit output voltage ripple and input and output capacitor ESR losses. Also if the RMS currents through the capacitors are larger than their rated value, the lives of the capacitors will be reduced. Based on theoretical analysis and simulations, the minimum output capacitance that meets a worst case ±1% voltage regulation and also does not exceed the capacitor RMS current limit is 47 µF, and the minimum input capacitance that does not exceed RMS current limit is 4.4 mF. Hence, a 47 µF electrolytic capacitor and two 2.2 mF electrolytic capacitors are used as output and input capacitors, respectively.

D. ZVS Operation

As described in Section II, the switching frequency of the ICN converter needs to be slightly higher than the resonant frequency of the resonant tank to ensure ZVS operation of the inverter transistors across the converter's full operating range. To determine the appropriate switching frequency, the designed ICN converters have been simulated at different switching frequencies across the entire operating range, and the simulated waveforms used to determine whether ZVS operation is achieved at all these operating points. For instance, consider a high-to-low transition of the inverter output voltage, as shown in Fig. 12(a). During this transition, the inverter output current needs to be positive enough to fully discharge the output capacitance of the bottom transistor (C_{ds2} in Fig. 12(a)), while simultaneously charging the output capacitance of the top transistor (C_{ds1} in Fig. 12(a)). The maximum charge that the inverter output current can move from the output capacitances can be obtained by integrating the inverter output current from the transistor turnoff instant to the current zero-crossing. This is referred to as the maximum movable charge in Fig. 12(b). To achieve ZVS operation, the maximum movable charge needs to be greater than or equal to the charge that needs to be moved. Similar analysis applies to the low-to-high transitions of the inverter output voltage.

The maximum movable charge and the charge that needs to be moved for the medium-Q ICN converter are plotted as a function of input voltage in Fig. 13 for the two extreme values of output voltage: 250 V and 400 V. As can be seen from Fig. 13, the maximum movable charge for both the top and bottom

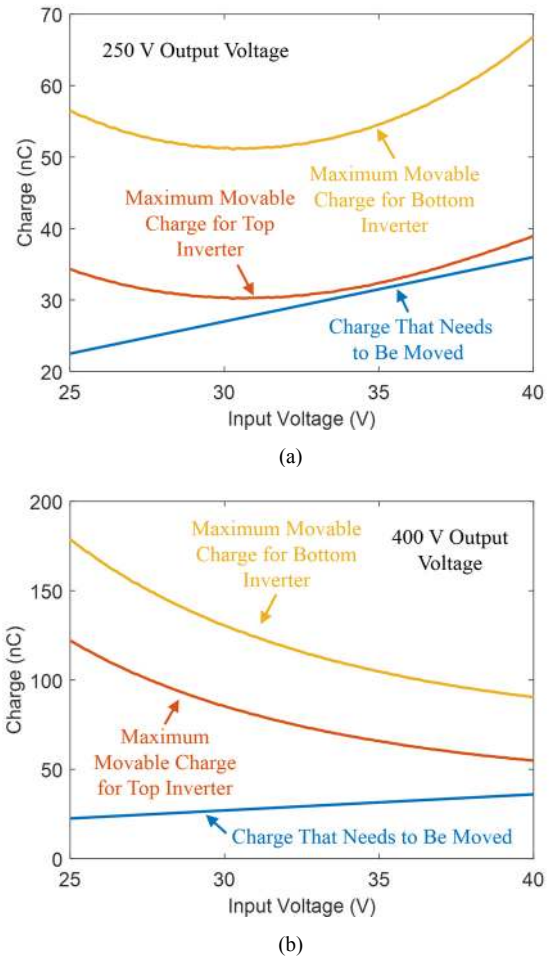

Fig. 13. Maximum movable charge and charge that needs to be moved for the top and bottom inverters (as shown in Fig. 4) of the medium-Q ICN converter as a function of input voltage for two extreme output voltage cases: (a) output voltage equal to 250 V and (b) output voltage equal to 400 V. These plots are obtained from the simulated waveforms of the medium-Q ICN converter switching at 509 kHz.

inverters (as shown in Fig. 4) is always larger than the charge that needs to be moved when the switching frequency is increased to 509 kHz. Hence, the medium-Q ICN converter can achieve ZVS operation across its entire operating range at a switching frequency of 509 kHz. Using similar analysis, the switching frequency needed to guarantee ZVS operation for the high-Q design is found to be roughly the same as that for the medium-Q design. However, the required switching frequency for the low-Q design is slightly higher. This is because the current waveforms of the medium-Q and high-Q designs are both fairly sinusoidal, while the currents of the low-Q design have substantial harmonic content.

IV. Experimental Results

The low-Q, medium-Q and high-Q 200-W prototype ICN converters have been built and tested. All three converters are operated at a switching frequency of 505 kHz, slightly higher than the designed switching frequency, to make the two inverters sufficiently inductively-loaded to achieve zero voltage switching (ZVS). Although this switching frequency is slighlty lower than the theoratically predicited value in Section III-D, it is sufficient to achieve ZVS operation across the entire operating range of the converters. This is partly because the theoretical model assumes a fixed value for the output capacitance of the inverter transistors, while the actual transistors' output capacitance has a strong nonlinear dependence on voltage.

A. ZVS, Near ZCS and Burst Mode Operation

Figure 14 shows the measured waveforms of the three ICN converters when operated at full power (200 W) at their minimum input voltage (V_{IN} = 25 V) and minimum output voltage (V_{OUT} = 250 V). To deliver full power at these voltages, burst mode (on/off) control is not needed, as the converters produce 200 W of output power when they are running continuously. Clearly the switches of both the top and the bottom inverters of the three converters achieve ZVS and near

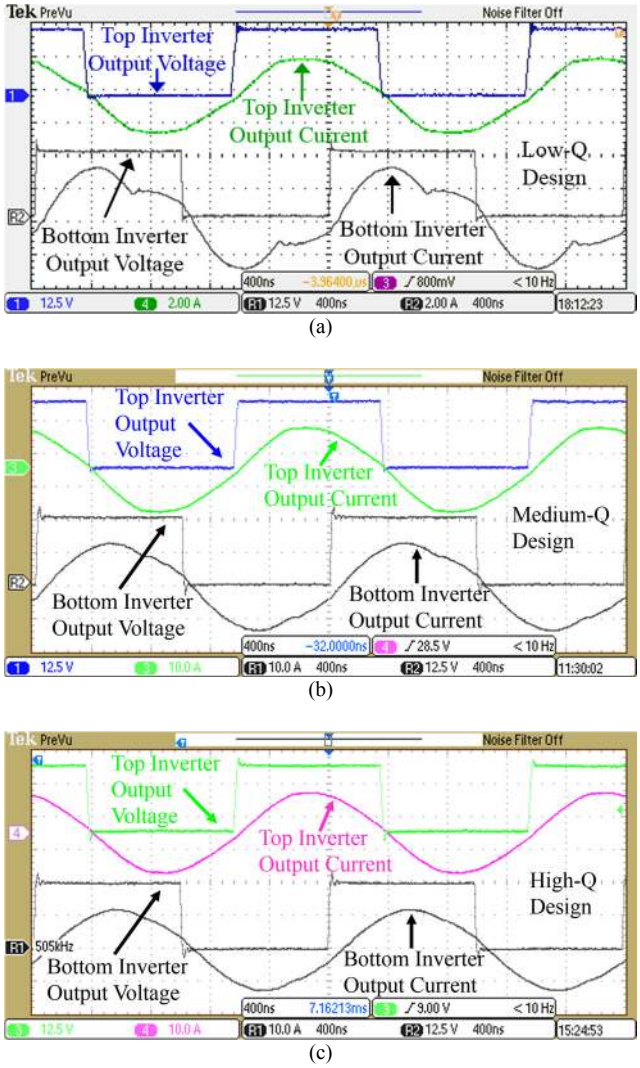

Fig. 14. Measured waveforms for the (a) low-Q, (b) medium-Q and (c) high-Q ICN converters operating at full power (200 W) at 25 V input voltage and 250 V output voltage. Waveforms shown are the output voltage and output current of both (top and bottom) half-bridge inverters of the (a) low-Q ICN converter, (b) medium-Q ICN converter and (c) high-Q ICN converter.

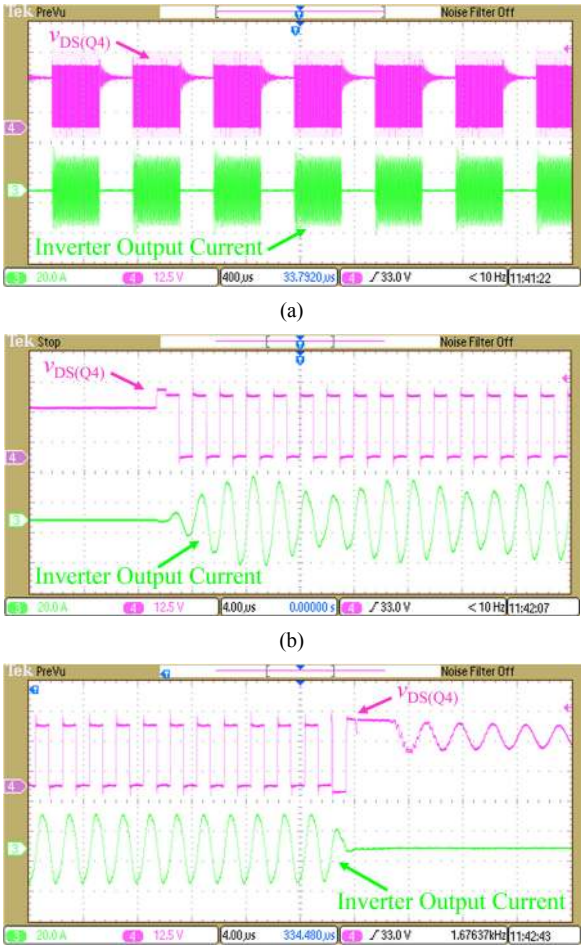

(a)

(b)

(c)

Fig. 15. Burst mode operation of the medium-Q ICN resonant converter delivering full power (200 W) at 25 V input voltage and 400 V output voltage. Waveforms shown are the output voltage and output current of the bottom half-bridge inverter: (a) long timescale showing multiple startup and shutdown sequences, (b) zoomed timescale to show the startup dynamics, and (c) zoomed timescale to show the shutdown dynamics.

ZCS. ZVS is achieved as the inverter output current is sufficiently negative during the low to high inverter output voltage transitions and sufficiently positive during the high to low inverter output voltage transitions. Near ZCS is achieved as the currents are fairly sinusoidal (due to the presence of the series resonant tanks with reasonable loaded quality factors), with phase that only slightly lags the voltage waveforms.

A useful measure of near ZCS operation is the ratio of the switch current at turn-off to its peak current. For the low-Q converter, the turn-off current of the top inverter is about 1.5 A, which is about 17% of the peak current value; the turn-off current of the bottom inverter is about 2.7 A, which is about 19% of the peak value of the current. The medium-Q and high-Q converters have similar performance in terms of near ZCS operation, even though they use quality factors that are at least three times larger than the low-Q version. The ratios of the turn-off switch current to the peak current for the medium-Q converter are 16% for the top inverter and 25% for the bottom one, and the ratios of the turn-off switch current to the peak current for the high-Q converter are 18% for the top inverter and 30% for the bottom one.

The waveforms of Fig. 14 can also be used to compare the theoretically-required phase shift between the two inverters and that needed in practice to achieve ZVS and near ZCS operation. In Fig. 14 the phase shift between the two inverters is about 634 ns for the three converters, which is 32% of the switching period (1.982 μs) and corresponds to an angle of 115.16°. This is within 0.5% of the theoretically predicted phase shift value (115.58°) calculated using (2).

When the output voltage and - to a lesser extent - the input voltage of the converter increase above their minimum values, burst mode control is needed to limit output power to 200 W (see Fig. 7). Burst mode control is also needed at all input/output voltage combinations when the output power is reduced below 200 W. Figure 15 shows the operation of the medium-Q converter under burst mode control with an input voltage of 25 V, an output voltage of 400 V and the output power regulated to 200 W. Fixed-frequency PWM burst-mode on/off modulation was used, with a bursting frequency of 1.68 kHz. This value is selected as it provides a good balance between the additional losses in the input capacitors due to the on/off modulation frequency ripple current and the additional losses in the converter due to its repeated startup and shutdown. Figure 15 also shows zoomed-in views of the bottom inverter's output voltage and output current waveforms during converter startup and shutdown. As stated in Section III, large output capacitance is needed to achieve good output voltage regulation when the converter is operating in burst mode. To verify the output voltage regulation of the prototype ICN converters, the output votlage ripple is measured when the converters are operating with 40 V input voltage, 400 V output voltage and 200 W output power. The output voltage of the low-Q converter

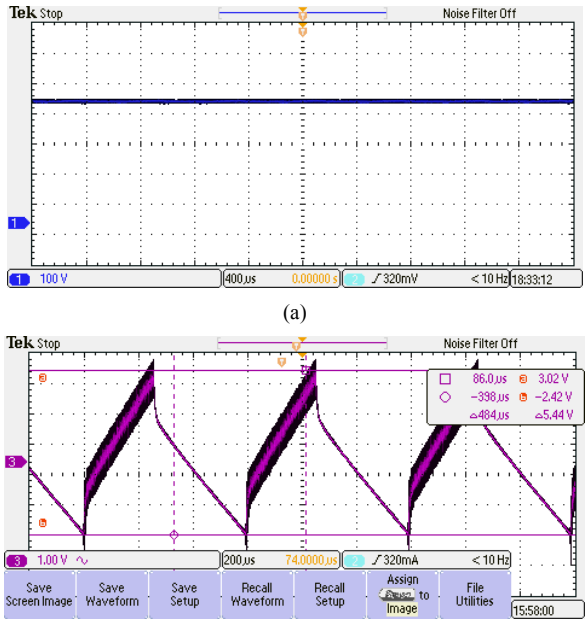

(a)

(b)

Fig. 16. Output voltage for the low-Q ICN converter operating with 40 V input voltage, 400 V output voltage, and 200 W output power measured in (a) 100 V/division and (b) 1 V/division.

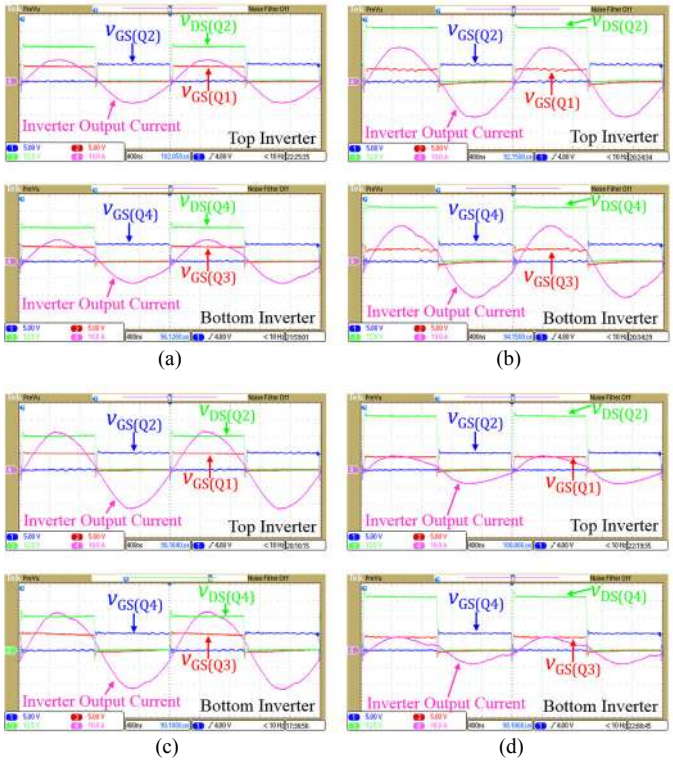

Fig. 17. Measured waveforms confirming ZVS and near ZCS operation of the medium-Q ICN resonant converter at four extreme operating points in terms of input voltage (V_{IN}) and output voltage (V_{OUT}): (a) V_{IN} = 25 V, V_{OUT} = 250 V, (b) V_{IN} = 40 V, V_{OUT} = 400 V, (c) V_{IN} = 25 V, V_{OUT} = 400 V, (d) V_{IN} = 40 V, V_{OUT} = 250 V.

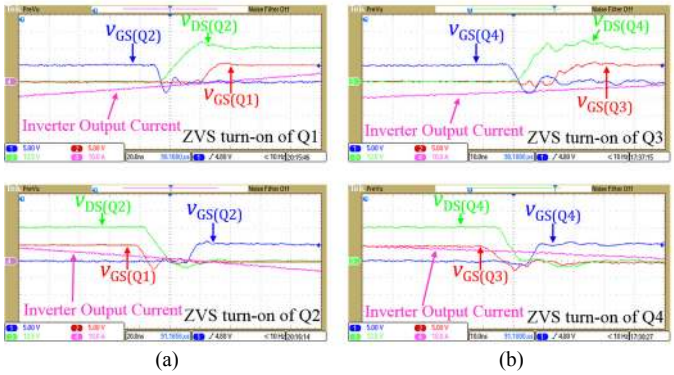

Fig. 18. Measured waveforms confirming ZVS operation of the medium-Q ICN resonant converter with V_{IN} = 25 V, V_{OUT} = 400 V: (a) ZVS turn-on of the transistors in the top inverter and (b) ZVS turn-on of the transistors in the bottom inverter.

is shown in Fig. 16 at this operating point. As can be seen from Fig. 16, the output voltage is quite flat and its ripple has a peak-to-peak value of 5.44 V, which is equivalent to ±0.68% and within the designed range.

To validate that the ICN resonant converter achieves ZVS and near ZCS operation across its entire design range, the operation of the low-Q, medium-Q and the high-Q ICN converters has been tested across their specified input voltage, output voltage and output power ranges. Figure 17 shows the pertinent waveforms of the medium-Q converter at four extreme operating points as input voltage is varied from 25 V to 40 V and output voltage is varied from 250 V to 400 V, while keeping output power constant at 200 W. Again it is easy to see that both (top and bottom) inverters of the ICN converter achieve ZVS turn-on and near ZCS turn-off at all four operating points. Figure 18 shows the zoomed in view of the switch voltages and currents during the switching transitions when operating with 25 V input and 400 V output. The ZVS turn-on of all the transistors can be observed in Fig. 18. It has been confirmed that the medium-Q ICN converter achieves ZVS and near ZCS operation across its entire operating range. Similarly the ZVS and near ZCS operation of the low-Q and high-Q converter has been confirmed across the entire operating range. In Fig. 17, it can also be found that the phase lag of the inverter output current relative to the inverter output voltage is different for different operating points. This is because the needed phase lag of the inverter output current depends on the charge (determined by the input voltage) that has to be moved from the output capacitances of the inverter switches and the available current (determined by the maximum output power) to allow this to happen.

B. Efficiency Comparison

The efficiency of the three prototype ICN converters has been measured across their entire operating range. The measured efficiency of the three converters is plotted in Fig. 19 across variations in input voltage, output voltage and output power. Note that all the efficiency plots are fairly flat.

Figure 19(a) and (b) plot the efficiency of the ICN converters as their input voltage is varied from 25 V to 40 V, while the output voltage and output power are held constant. In both cases the output power is 200 W, while the output voltage is 250 V in Fig. 19(a) and 400 V in Fig. 19(b). When the output voltage is 250 V, the peak efficiency of the low-Q ICN converter is 97.1% and its efficiency does not fall below 96.4% as the input voltage is varied across its entire range. The efficiency increases monotonically with increasing input voltage, as primary-side conduction losses are reduced with decreasing input current. The medium-Q converter has a slightly higher peak efficiency of 97.2% and the high-Q converter has a slightly lower peak efficiency of 96.8% than the low-Q converter, but the shapes of the efficiency plots are similar. The efficiency of the converters reduces at higher output voltages, as the converters have to be operated in burst mode to limit output power. However, at full output power (200 W) the efficiency of the low-Q converter never falls below 95%, which occurs at the lowest input voltage (25 V) and highest output voltage (400 V). This is also the operating point at which the difference in efficiency between the low-Q and the high-Q designs is the largest (2.1%). This is because at this operating point the converter has the highest input current resulting in large conduction losses in the inductors.

Figure 19(c) and (d) plot the efficiency of the three ICN converters as their output voltage is varied from 250 V to 400 V, while the input voltage and output power are held constant. Again in both cases output power is 200 W, while input voltage is 25 V in Fig. 19(c) and 40 V in Fig. 19(d). When the input voltage is 40 V, the efficiency of the low-Q converter stays

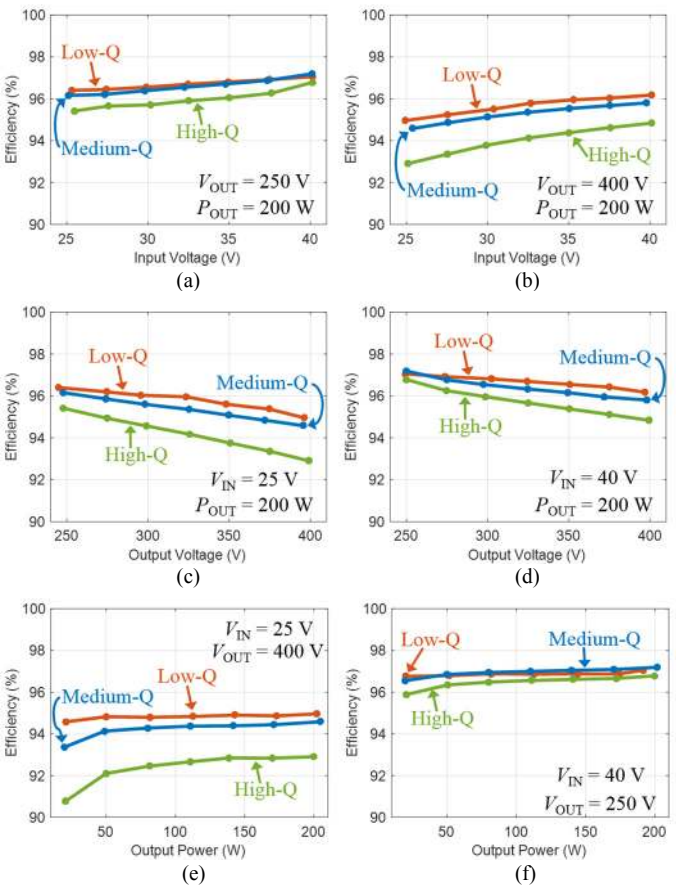

Fig. 19. Measured efficiency of the low-Q, medium-Q and high-Q ICN resonant converters across variations in input voltage (V_{IN}), output voltage (V_{OUT}) and output power (P_{OUT}): (a) variation in input voltage with V_{OUT} = 250 V and P_{OUT} = 200 W, (b) variation in input voltage with V_{OUT} = 400 V and P_{OUT} = 200 W, (c) variation in output voltage with V_{IN} = 25 V and P_{OUT} = 200 W, (d) variation in output voltage with V_{IN} = 40 V and P_{OUT} = 200 W, (e) variation in output power with V_{IN} = 25 V and V_{OUT} = 400 V, and (f) variation in output power with V_{IN} = 40 V and V_{OUT} = 250 V.

above 96.2% and achieves a peak value of 97.1% when the output voltage is at its minimum (250 V). Again the worst case efficiency of the low-Q converter is 95%, at minimum input voltage (25 V) and maximum output voltage (400 V). The efficiency of the high-Q design is again lower than that of the low-Q and medium-Q designs.

The efficiency of the three ICN converters as the output power is varied is plotted in Fig. 19(e) and (f). In Fig. 19 (e) the input voltage is held at 25 V and the output voltage is held at 400 V and in Fig. 19(f) the input voltage is held at 40 V and the output voltage is held at 250 V. In both cases burst mode control is used to vary the output power from 20 W to 200 W. The efficiency of the three converters as a function of output power is quite flat, varying by only 0.3% for the low-Q design over its entire 10:1 output power range when input voltage is 40 V and output voltage is 250 V. The low-Q converter has its lowest efficiency of 94.6% when input voltage is at its minimum (25 V), output voltage is at its maximum (400 V) and output power is at its minimum (20 W). When input voltage is 40 V and output voltage is 250 V the peak efficiency is 97.1% at an output power of 200 W and the efficiency is still above 96.8% at an output power of 20 W. Hence, burst mode control is a good method for regulating output power in an ICN resonant converter as it enables good light load efficiency. However, it does require larger input and output capacitors than might otherwise be used (depending upon the application). For the low-Q ICN converter, the efficiency at 10% of rated power is only 1.2% lower than its full load efficiency, but requires the addition of a 47-uF/450-V electrolytic cpacitor with volume of 0.28 in^3.

In summary, the low-Q ICN converter has higher efficiency than the higher Q designs across the full operating range, except for a narrow range around the 40 V input voltage and 250 V output voltage operating point, where the medium-Q design has the highest efficiency. Both the low-Q and medium-Q designs have higher efficiency than the high-Q converter across the full operating range. This is because the low-Q and medium-Q converters have significantly lower conduction losses due to their lower valued inductors, and they are still able to maintain ZVS and near ZCS operation across the full operating range. The average values of the full-power efficiencies at the four corner operating points are calculated for each prototype converter and plotted in Fig. 20. As can be seen from Fig. 20, there is a good match between the experimental and the theoretically predicted efficiencies.

The efficiency results presented above demonstrate that the ICN resonant converter is able to maintain very high efficiencies across a wide range of operating conditions in terms of input voltage, output voltage and output power. To better understand the tradeoffs between the low-Q and the high-Q designs, and explore opportunities for further improvements in efficiency of the ICN converter, a loss breakdown analysis of the three converters has been performed based on the analytical models of the individual loss mechanisms given in Appendix B. Figure 21 shows the estimated loss breakdown of the three ICN converters when operating at 32.5 V input voltage, 325 V output voltage and 200 W output power. At this operating point, the diode, magnetic, and transistor losses account for the majority of the power losses for all the three converters. For the

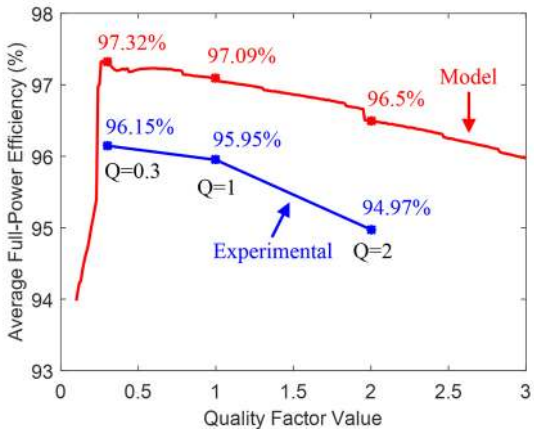

Fig. 20. Experimental and theoretically predicted average full-power efficiencies of ICN converters versus their Q value. In all converters, the switching frequency is 505 kHz.

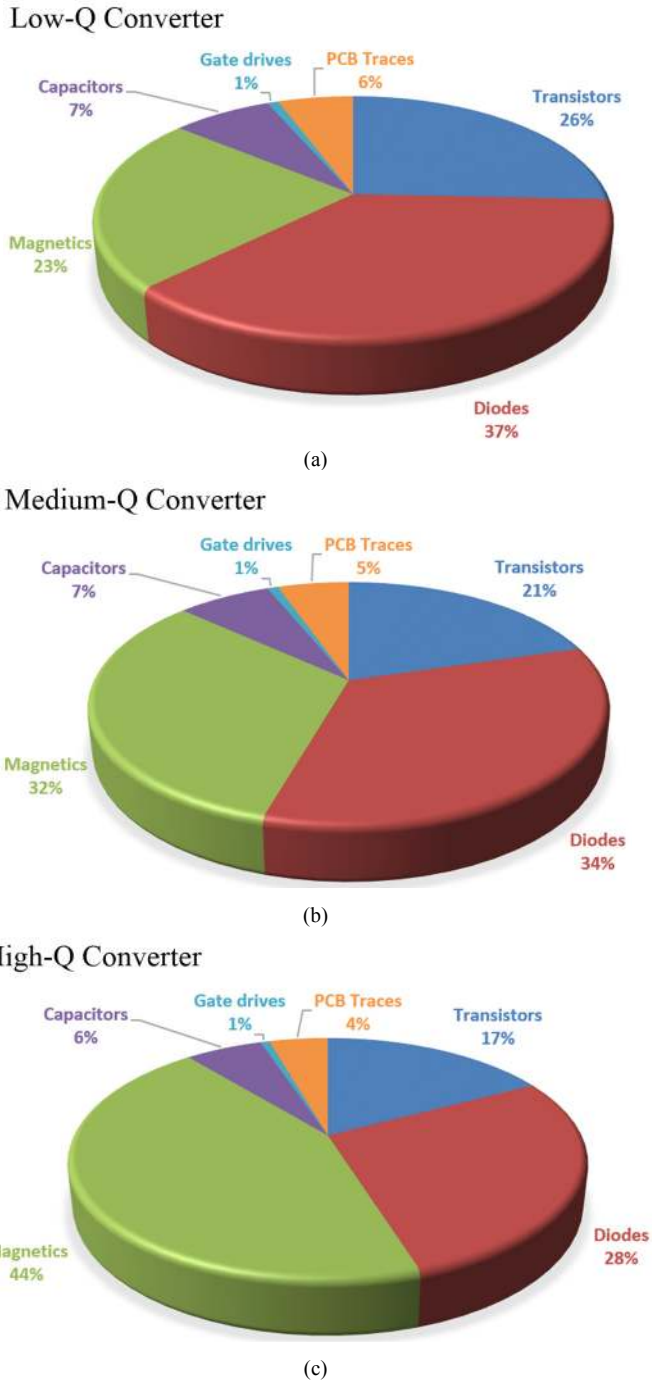

Fig. 21. Loss breakdown of (a) low-Q, (b) medium-Q and (c) high-Q ICN converter based on theoretical models when the converters are operating at an input voltage of 32.5 V, output voltage of 325 V and output power of 200 W.

low-Q design, the transistor losses are larger than the magnetic losses. For the medium-Q design, the magnetic losses are slightly larger than the transistor losses, while in the high-Q design the magnetic losses are much larger than the transistor losses. In all converters, there are also some losses in the resonant and bypass capacitors and the PCB traces. The gate drive losses are very small due to the use of low gate charge GaN transistors. Figure 22 compares the measured and the

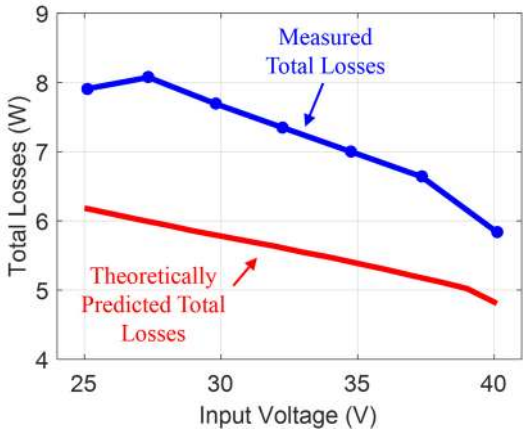

Fig. 22. Comparison of measured and theoretically predicted total losses in the medium-Q ICN converter as a function of input voltage when the converter is operating at an output voltage of 250 V and output power of 200 W.

theoretically predicted total losses in the medium-Q ICN converter across its full input voltage range when operating at 250 V output voltage and 200 W output power. There is reasonably good agreement between the predicted and measured values.

V. Conclusions

This paper presents a new resonant converter architecture that utilizes an impedance control network (ICN) to maintain zero-voltage switching (ZVS) and near zero-current switching (ZCS) across wide operating ranges in terms of input and output voltages and output power. Three prototype 200 W, 500 kHz ICN resonant converters, one with low-Q, another with medium-Q and the third one with high-Q resonant tanks, designed to operate over an input voltage range of 25 V to 40 V and an output voltage range of 250 V to 400 V are built and tested. The low-Q prototype ICN converter achieves a peak efficiency of 97.1%, maintains greater than 96.4% full power efficiency at 250 V output voltage across the nearly 2:1 input voltage range, and maintains full power efficiency above 95% across its full input and output voltage range. It also maintains efficiency above 94.6% over a 10:1 output power range across its full input and output voltage range owing to the use of burst-mode control.

Acknowledgement

The authors wish to acknowledge the financial support received from the National Science Foundation (NSF) under Award Number 1307699.

Appendix A – Effective Admittance and Output Power of ICN Converter

This appendix derives the expression for the effective admittances seen by the two inverters (Y_1 and Y_2), as given by (1), and the expression for the output power of the ICN

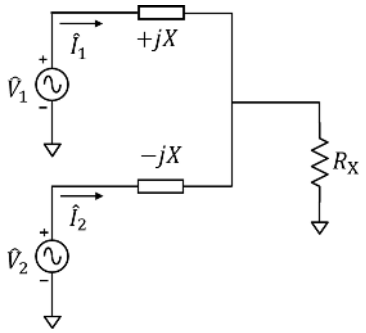

Fig. 23. An equivalent circuit model for the ICN converter of Fig. 4 under fundamental frequency approximation. The two input branches of the impedance control network have equal but opposite reactances ($+jX$ and $-jX$). $\hat{V}_1$ and $\hat{V}_2$ are the fundamental components of the output voltages of the inverters, $\hat{I}_1$ and $\hat{I}_2$ are the fundamental components of the output currents of the inverters, and R_X is the equivalent resistance of the rectifier referred to the primary side of the transformer.

converter under fundamental frequency approximation, as given by (3).

Figure 23 shows an equivalent circuit model for the ICN converter of Fig. 4 under fundamental frequency approximation. In this model, $\hat{V}_1$ and $\hat{V}_2$ are the fundamental components of the output voltages of the inverters, $\hat{I}_1$ and $\hat{I}_2$ are the fundamental components of the output currents of the inverters, and R_x is the equivalent resistance of the rectifier referred to the primary side of the transformer. The expressions for $\hat{V}_1$, $\hat{V}_2$ and R_x are given below:

$$\hat{V}_1 = \frac{2}{\pi} V_{IN} e^{j\Delta}, \tag{10}$$

$$\hat{V}_2 = \frac{2}{\pi} V_{IN} e^{-j\Delta}, \tag{11}$$

$$R_X = \frac{2V_{OUT}^2}{\pi^2 N^2 P_{OUT}}. \tag{12}$$

Here V_{IN} is the input voltage, V_{OUT} is the output voltage, P_{OUT} is the output power, N is the transformer turns ratio, and 2Δ is the phase shift between the two inverters. The expressions for $\hat{I}_1$ and $\hat{I}_2$ can be derived using superposition:

$$\hat{I}_1 = \frac{R_X - jX}{X^2}\hat{V}_1 - \frac{R_X}{X^2}\hat{V}_2, \tag{13}$$

$$\hat{I}_2 = \frac{R_X + jX}{X^2}\hat{V}_2 - \frac{R_X}{X^2}\hat{V}_1. \tag{14}$$

Hence, the effective admittances seen by the two inverters are given by:

$$Y_1 \equiv \frac{\hat{I}_1}{\hat{V}_1} = \frac{R_X - jX}{X^2} - \frac{R_X}{X^2} e^{-j2\Delta}, \tag{15}$$

$$Y_2 \equiv \frac{\hat{I}_2}{\hat{V}_2} = \frac{R_X + jX}{X^2} - \frac{R_X}{X^2} e^{j2\Delta}. \tag{16}$$

Here, R_x is an unknown that can be eliminated using (12) and an additional expression relating R_x and output power, as follows. Assuming a lossless converter, output power is equal to input power:

$$\begin{aligned} P_{OUT} = P_{IN} &= \mathrm{Re}\left\{\frac{1}{2}\hat{V}_1\hat{V}_1^* Y_1^* + \frac{1}{2}\hat{V}_2\hat{V}_2^* Y_2^*\right\} \\ &= \left(\frac{2}{\pi}V_{IN}\right)^2 \frac{R_X}{X^2}(1-\cos 2\Delta). \end{aligned} \tag{17}$$

Combining (12) and (17) yields an expression for R_x that is in terms of given quantities:

$$R_X = \frac{V_{OUT} X}{2NV_{IN}\sin\Delta}. \tag{18}$$

Substituting (18) into (15) and (16) gives the desired expression for the effective admittances seen by the two inverters, which is the same as (1):

$$Y_1 = Y_2^* = \frac{V_{OUT}\sin\Delta}{NV_{IN}X} + j\left(\frac{V_{OUT}\cos\Delta}{NV_{IN}X} - \frac{1}{X}\right). \tag{19}$$

Now, substituting R_x, as given by (18), into the expression for output power, as given by (17), gives:

$$P_{OUT} = \frac{4V_{IN}V_{OUT}\sin\Delta}{\pi^2 NX}. \tag{20}$$

The effective susceptance seen by both inverters is zero when the phase shift between them is given by:

$$2\Delta = 2\cos^{-1}\left(\frac{NV_{IN}}{V_{OUT}}\right). \tag{21}$$

Substituting (21) into (20) yields the desired expression for the output power of the ICN converter when operated with both inverters seeing zero effective susceptance, which is the same as (3):

$$P_{OUT} = \frac{4V_{IN}\sqrt{V_{OUT}^2 - N^2V_{IN}^2}}{\pi^2 NX}. \tag{22}$$

Appendix B – Loss Model

This appendix provides the loss model that is used to estimate the efficiency and loss breakdown of the ICN converter. This loss model includes transistor losses, diode losses, inductor losses, transformer losses, capacitor losses, and the PCB trace losses. The equations used to estimate the losses are summarized below.

Inverter Losses:

The turn-on losses of the transistors in the inverters are negligible as they achieve ZVS at all operating points. Therefore, only conduction losses, turn-off losses and gate charge losses are considered for these transistors. The conduction losses in each transistor are calculated using:

$$P_{trans,cond} = I_{rms}^2 R_{ds(on)}, \tag{23}$$

where, I_{rms} is the RMS current through the transistor, $R_{ds(on)}$ is the on-state resistance of the transistor. The turn-off losses of each transistor are calculated assuming the current through its channel decreases linearly to zero upon transistor turns off. The remaining current (which increases linearly) flows into its output capacitance, leading to a quadratic rise in the transistor's drain-source voltage. The overlap between the channel current and the drain-source voltage results in losses, and is given by:

$$P_{\text{trans,off}} = \frac{I_{\text{off}}^2 t_{\text{off}}^2 f_{\text{sw}}}{48 C_{\text{oss}}}. \quad (24)$$

Here I_{off} is the current through the transistor at the turn-off instant, t_{off} is the fall time of the current, f_{sw} is the switching frequency of the converter, and C_{oss} is the output capacitance of the transistor. The gate charge losses of each transistor are calculated using:

$$P_{\text{trans,gate}} = V_{\text{gs}} Q_{\text{g}} f_{\text{sw}}, \quad (25)$$

where V_{gs} is the gate-to-source voltage of the transistor, and Q_{g} is the total gate charge of the transistor.

Rectifier Losses:

The rectifier diode in on-state can be modeled as a voltage source in series with an on-state resistor. Therefore, diode losses are calculated using:

$$P_{\text{diode}} = I_{\text{avg}} V_{\text{t}} + I_{\text{rms}}^2 R_{\text{t}}, \quad (26)$$

where I_{avg} is the average current through the diode, V_{t} is the diode's voltage drop, I_{rms} is the RMS current through the diode, and R_{t} is its on-state resistance.

Magnetic Losses:

Losses in the inductors and the transformer include winding losses and core losses. Winding losses are calculated using:

$$P_{\text{winding}} = \sum_{i=1}^{11} I_{\text{rms},i}^2 R_{\text{dc}} F_{\text{r},i}, \quad (27)$$

where $I_{\text{rms},i}$ is the RMS value of the ith harmonic of the current through the winding, R_{dc} is the dc resistance of the winding, and $F_{\text{r},i}$ is a factor that relates the ac resistance to the dc resistance, and is determined using equation (2) of reference [21]. The first eleven harmonics of the winding current are used to calculate the winding losses. The core losses are calculated using the improved generalized Steinmetz equation (iGSE) [22]:

$$P_{\text{core}} = V_{\text{c}} \frac{1}{T} \int_0^T k_i \left| \frac{\text{d}B}{\text{d}t} \right|^{\alpha} (\Delta B)^{\beta-\alpha} \text{d}t, \quad (28)$$

$$k_i = \frac{k}{(2\pi)^{\alpha-1} \int_0^{2\pi} |\cos\theta|^{\alpha} 2^{\beta-\alpha} \text{d}\theta}. \quad (29)$$

Here V_{c} is the core volume, B is the flux density, ΔB is the peak-to-peak flux density, T is the cycle period of the flux density (the same as switching period), and k, α and β are material parameters used in the basic Steinmetz equation $P_{\text{v}} = k f^{\alpha} B_{\text{pk}}^{\beta}$, where P_{v} is the core loss per unit volume, and B_{pk} is the peak value of a sinusoidal excitation, and f is the frequency of the sinusoidal excitation.

Capacitor Losses:

The losses in the capacitors are calculated using:

$$P_{\text{cap}} = I_{\text{rms}}^2 R_{\text{esr}}, \quad (30)$$

where I_{rms} is the RMS current through the capacitor, and R_{esr} is the equivalent series resistance of the capacitor.

PCB Trace Losses:

The PCB trace losses are calculated using:

$$P_{\text{PCB}} = I_{\text{rms}}^2 R_{\text{dc}} \frac{h}{\delta}, \quad (31)$$

where I_{rms} is the RMS current through the PCB trace, R_{dc} is the dc resistance of the PCB trace, h is the thickness of the trace, and δ is the skin depth.

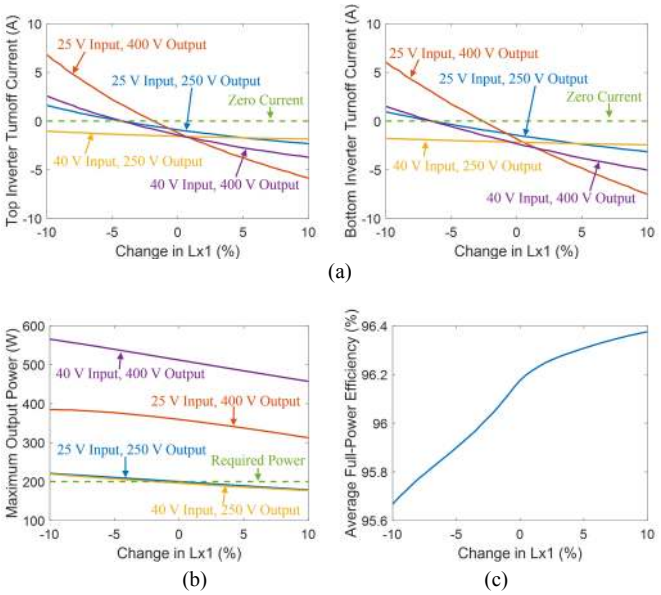

Fig. 24. Variations in (a) inverter turn-off current, (b) maximum output power, and (c) average full-power efficiency of the medium-Q (Q=1) ICN converter as a function of variations in L_{X1}.

Appendix C – Sensitivity Analysis

To investigate the robustness of the ICN converter to variations in component values, and the possibility of compensating for these variations through slight changes in the available control handles, the sensitivity of the ICN converter's key performance metrics to variations in component values, switching frequency, and the phase shift between the inverters is studied. The performance metrics of interest are the converter's soft switching ability, maximum output power, and conversion efficiency. The change in these performance metrics as the value of inductor L_{X1} varies across a ±10% range is shown in Fig. 24. As can be seen from Fig. 24 (a), the sensitivity of the inverter turnoff current to variations in in value of L_{X1} depends on the converter's operating point. The inverter turnoff current for both inverters is most sensitive when the ICN converter is at its maximum boost operating point (25 V input voltage and 400 V output voltage). At all operating points the inverter turnoff current tends towards a positive value when the value of L_{X1} decreases, and with a large decrease in L_{X1} the inverter switches will lose ZVS. At the worst case operating point (25 V input voltage and 400 V output voltage) the loss in ZVS occurs when L_{X1} is reduced by around 2.5% from its nominal value. When the value of L_{X1} increases, the inverter turnoff current becomes more negative, which leads to the eventual loss of near ZCS. Interestingly the maximum output power and the efficiency of the ICN converter do not change too much across a ±10% variation in the value of L_{X1}. The change in performance of the ICN converter with variations in the values of the other components (C_{X1}, L_{X2}, C_{X2}, L_{r}, C_{r}) is also investigated in the same way. Figure 25 shows the change in the

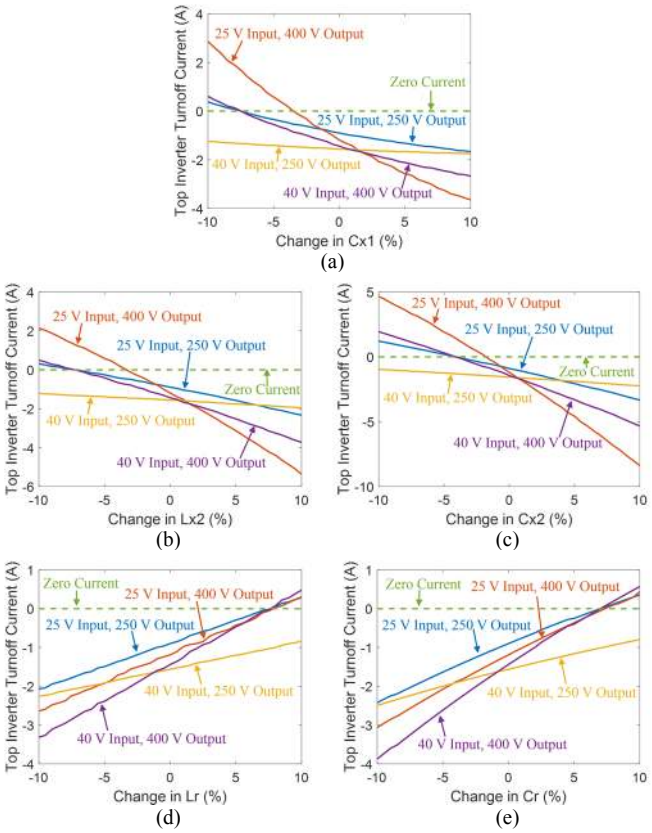

Fig. 25. Change in top inverter turnoff current of the medium-Q ICN converter across ±10% variations in the value of a) C_{X1}, (b) L_{X2}, (c) C_{X2}, (d) L_r, and (e) C_r.

top inverter turnoff current across ±10% variations in the values of these components. The top inverter turnoff current tends to become less negative when C_{X1}, L_{X2}, or C_{X2} decrease or when L_r or C_r increase, and the top inverter turnoff current becomes more negative when the component values change in the opposite direction. The change in the bottom inverter turnoff current is very similar to that in the top inverter. Also, as with variations in L_{X1}, the maximum output power and efficiency of the ICN converter do not change much with slight changes in these component values.

As shown above, variations in component values do change the soft switching ability of the ICN converter; therefore it is valuable to see if the available control handles (switching frequency and phase shift between inverters) can be adjusted slightly to compensate for the change in turn-off current. Figure 26 shows the change in performance of the ICN converter across ±5% variations in switching frequency. As can be seen from Fig. 26 (a), the inverter turnoff current is quite sensitive to the switching frequency. The inverter turnoff current will become less negative (and eventually positive) when the switching frequency decreases, and it will become more negative when switching frequency increases. Moreover, the change in maximum output power and efficiency is quite small with such variations in the switching frequency, as shown in Fig. 26 (b) and (c). Hence, switching frequency is a good candidate to compensate for changes in inverter turn-off

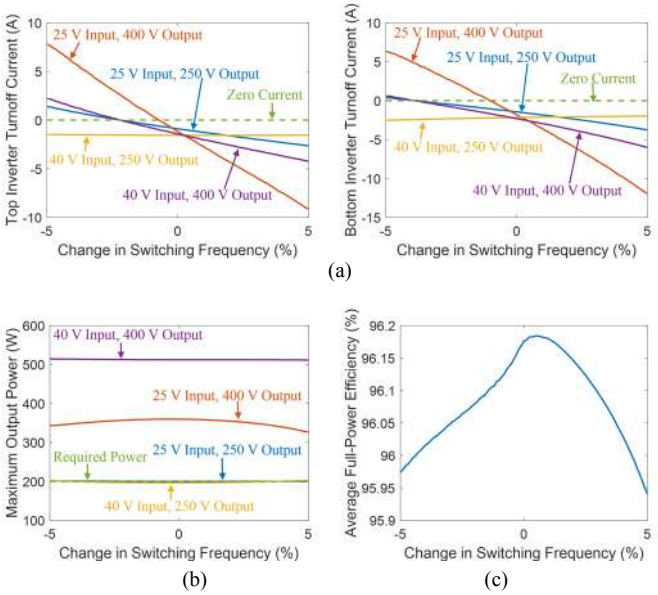

Fig. 26. Variations in (a) inverter turn-off current, (b) maximum output power, and (c) average full-power efficiency of the medium-Q (Q=1) ICN converter as a function of variations in switching frequency.

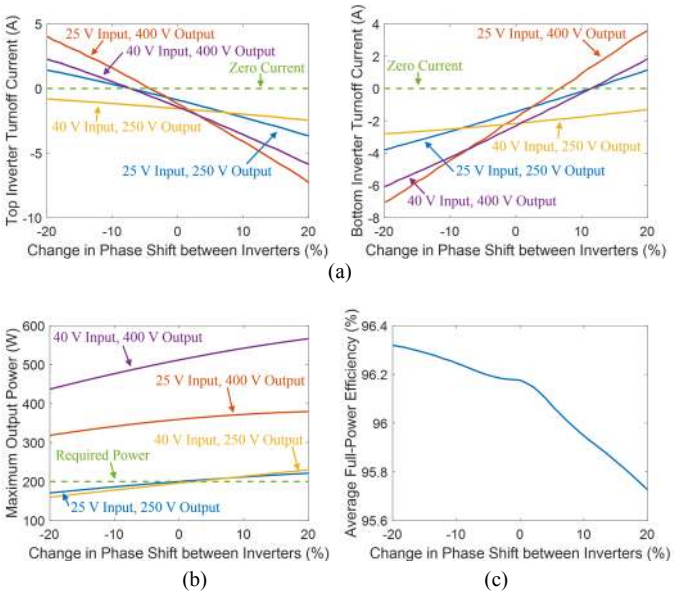

Fig. 27. Variations in (a) inverter turn-off current, (b) maximum output power, and (c) average full-power efficiency of the medium-Q (Q=1) ICN converter as a function of variations in phase shift.

currents and recover the soft switching ability of the ICN converter in case it is lost due to variations in component values. Another potential candidate is the phase shift between the inverters. Figure 27 shows the change in performance of the ICN converter across ±20% variations in phase shift between the inverters. As can be seen from Fig. 27 (a), the top and bottom inverter turnoff currents change in the opposite directions with variations in phase shift. Again, the change in maximum output power and efficiency is quite small with variations in phase shift, as can be seen in Fig. 27 (b) and (c). Hence, phase shift can be used to compensate for any

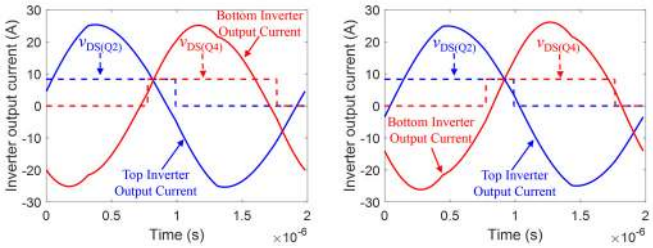

Fig. 28. Inverter output voltage and current for the medium-Q (Q=1) ICN converter with L_{X1} decreased by 10% from its original value. The switching frequencies used in (a) and (b) are 505 kHz and 525 kHz, respectively. In both cases, the converter is operated with 25 V input voltage and 400 V output voltage.

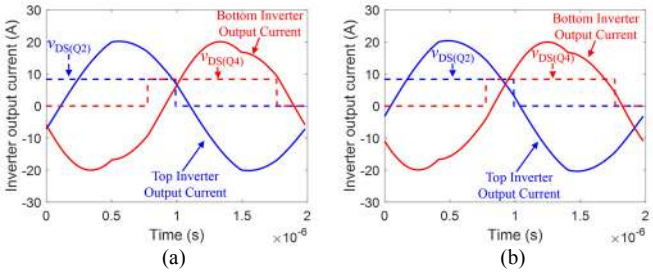

Fig. 29. Inverter output voltage and current for the medium-Q (Q=1) ICN converter with L_{X1} increased by 10% from its original value. The switching frequencies used in (a) and (b) are 505 kHz and 490 kHz, respectively. In both cases, the converter is operated with 25 V input voltage and 400 V output voltage.

differential-mode changes in the top and bottom inverter turnoff currents.

To demonstrate the above-mentioned compensation techniques for variations in inverter turn-off current due to variations in component values, two examples are considered. Figure 28 shows the inverter output voltage and current for the medium-Q ICN converter with L_{X1} decreased by 10% from its nominal value, while Fig. 29 shows the same waveforms with L_{X1} increased by 10% from its nominal value. In Fig. 28 (a), the switching frequency of the converter is 505 kHz, which results in positive turnoff current for both inverters, and both inverters lose ZVS. To recover ZVS capability, the switching frequency is increased by 4% (to 525 kHz) in Fig. 28 (b). The resultant inverter turn-off currents become slightly negative and both inverters achieve ZVS and near ZCS. In Fig. 29 (a) (with L_{X1} increased), the converter switches at 505 kHz, and the inverter turn-off currents are very negative so near ZCS is not achieved. In Fig. 29 (b), the switching frequency is decreased by 3% to 490 kHz to make the inverter turn-off current only slightly negative to achieve ZVS and near ZCS. Hence, slightly adjusting the switching frequency is an effective way to compensate for variations in the component values of the ICN converter. If L_{X1} had decreased and L_{X2} had increased, requiring a differential adjustment in the inverter currents, a slight adjustment in phase could additionally be employed to compensate for these changes.

The above discussion shows that with known component values, for a given combination of input and output voltages, there is an optimum choice of switching frequency and phase shift that results in a turnoff current which maximizes the converter efficiency. With known component values, one way to achieve this optimal turnoff current automatically would be to use a lookup table that stores the optimum values of switching frequency and phase shift as a function of input and output voltages. However, with component tolerances in a practical converter, the above method needs to be augmented with a self-learning algorithm that determines the optimum switching frequency and phase shift as a function of input and output voltages during converter operation to maximize efficiency. This can be achieved through an online efficiency optimization technique similar to the one presented in [23], [24].

REFERENCES

[1] R.L. Steigerwald, "High-Frequency Resonant Transistor DC-DC Converters," *IEEE Transactions on Industrial Electronics*, vol. IE-31, no. 2, pp. 181-191, May 1984.

[2] R.L. Steigerwald, "A Comparison of Half-Bridge Resonant Converter Topologies," *IEEE Transactions on Power Electronics*, vol. 3, no. 2, pp. 174-182, April 1988.

[3] J. Vandelac and P.D. Ziogas, "A DC to DC PWM Series Resonant Converter Operated at Resonant Frequency," *IEEE Transactions on Industrial Electronics*, vol. 35, no. 3, pp. 451-460, August 1988.

[4] M.Z. Youssef and P.K. Jain, "A Review and Performance Evaluation of Control Techniques in Resonant Converters," *Proceedings of the IEEE Industrial Electronics Society*, pp. 215-221, Busan, Korea, November, 2004.

[5] F.S. Tsai, P. Materu and F.C. Lee, "Constant-Frequency Clamped-Mode Resonant Converters," *IEEE Transactions on Power Electronics*, vol. 3, no. 4, pp. 460-473, October, 1988.

[6] P. Jain, A. St-Martin and G. Edwards, "Asymmetrical Pulse Width Modulated Resonant DC/DC Converter Topologies," *Proceedings of the IEEE Power Electronics Specialists Conference (PESC)*, pp. 818-825, Seattle, WA, June, 1993.

[7] J.M. Burdio, F. Canales, P.M. Barbosa and F.C. Lee, "A Comparison Study of Fixed-Frequency Control Strategies for ZVS DC/DC Series Resonant Converters," *Proceedings of the IEEE Power Electronics Specialists Conference (PESC)*, pp. 427-432, Vancouver, Canada, June, 2001.

[8] H. Chireix, "High Power Outphasing Modulation," Proceedings of the IRE, vol. 23, no.11, pp. 1370-1392, November 1935.

[9] Y. Han, O. Leitermann, D.A. Jackson, J.M. Rivas and D.J. Perreault, "Resistance Compression Networks for Radio-Frequency Power Conversion," *IEEE Transactions on Power Electronics*, pp. 41-53, January 2007.

[10] P.A. Godoy, D.J. Perreault, and J.L. Dawson, "Outphasing Energy Recovery Amplifier with Resistance Compression for Improved Efficiency, *IEEE Transactions on Microwave Theory and Techniques*, vol. 57, no. 12, pp. 2895-2906, December 2009.

[11] D.J. Perreault, "A New Power Combining and Outphasing Modulation System for High-Efficiency Power Amplification," *IEEE Transactions on Circuits and Systems – I,* vol. 58, no. 8, pp. 1713-1726, August 2011.

[12] A.S. Jurkov, L. Roslaniec and D.J. Perreault, "Lossless Multi-Way Power Combining and Outphasing for High-Frequency Resonant Inverters," *2012 International Power Electronics and Motion Control Conference*, pp. 910-917, June 2012.

[13] W. Inam, K.K. Afridi and D.J. Perreault, "High Efficiency Resonant DC/DC Converter Utilizing a Resistance Compression Network," *IEEE Transactions on Power Electronics*, pp. 4126-4135, vol. 29, no. 8, August 2014.

[14] T.W. Barton, J.L. Dawson and D.J. Perreault, "Experimental Validation of a Four-Way Outphasing Combiner for Microwave Power Amplification," *IEEE Microwave and Wireless Component Letters,* Vol. 23, No. 1, pp. 28-30, Jan. 2013.

[15] T.W. Barton and D.J. Perreault, "Four-Way Microstrip-Based Power Combining for Microwave Outphasing Power Amplifiers," *IEEE Transactions on Circuits and Systems - I,* Vol. 61, No. 10, pp. 2987-2998, October 2014.

[16] T.W. Barton, J. M. Gordonson, and D.J. Perreault, "Transmission Line Resistance Compression Networks and Applications to Wireless Power Transfer," *IEEE Journal of Emerging and Selected Topics in Power Electronics,* Vol. 3, No. 1, pp. 252 - 260, March 2015.

[17] Y. Lee and Y. Cheng, "A 580 kHz switching regulator using on-off control," *Journal of the Institution of Electronic and Radio Engineers*, vol. 57, no. 5, pp. 221–226, September/October 1987.

[18] R.C.N. Pilawa-Podgurski, A.D. Sagneri, J.M. Rivas, D.I. Anderson and D.J. Perreault, "High-Frequency Resonant Boost Converters," *IEEE Transactions on Power Electronics,* vol. 24, No. 6, pp. 1654-1665, June 2009.

[19] J. Hu, A.D. Sagneri, J.M. Rivas, Y. Han, S.M. Davis, and D.J. Perreault, "High-Frequency Resonant SEPIC Converter with Wide Input and Output Voltage Ranges," *IEEE Transactions on Power Electronics,* Vol. 27, No. 1, pp. 189-200, Jan. 2012.

[20] J. Lu, D.J. Perreault and K.K. Afridi, "Impedance Control Network Resonant dc-dc Converter for Wide-range High Efficiency Operation," *Proceedings of the IEEE Applied Power Electronics Conference and Exposition (APEC),* Charlotte, NC, March 2015.

[21] C. R. Sullivan, "Optimal Choice for Number of Strands in a Litz-Wire Transformer Winding", *IEEE Transactions on Power Electronics,* Vol. 14, No. 2, pp. 283-291, Mar. 1999.

[22] K. Venkatachalam, C. R. Sullivan, T. Abdallah, and H. Tacca, "Accurate prediction of ferrite core loss with nonsinusoidal waveforms using only Steinmetz parameters", *Proceedings of the IEEE Workshop on Computers in Power Electronics,* pp. 36–41, June 2002.

[23] L. Scandola, L. Corradini, G. Spiazzi, C. Garbossa, P. Piersimoni and A. Vecchiato, "Online Efficiency Optimization Technique for Digitally Controlled Resonant DC/DC Converters," *Proceedings of the IEEE Applied Power Electronics Conference and Exposition (APEC),* Fort Worth, TX, March 2014.

[24] A. Sepahvand, L. Scandola, Y. Zhang and D. Maksimovic, "Voltage Regulation and Efficiency Optimization in a 100 MHz Series Resonant DC-DC Converter," *Proceedings of the IEEE Applied Power Electronics Conference and Exposition (APEC),* Charlotte, NC, March 2015.

Jie Lu (S'14) received his B.Eng. degree in Automation from Harbin Institute of Technology, Harbin, China in 2012, and the M.S. degree in Electrical Engineering from University of Colorado Boulder, Boulder, CO, USA in 2015, where he is currently working towards a Ph.D. degree. His research interests include high frequency resonant converters, modeling and control of power electronics, and application of these in dc distribution systems.

David J. Perreault (S'91, M'97, SM '06, F'13) received the B.S. degree from Boston University, Boston, MA, and the S.M. and Ph.D. degrees from the Massachusetts Institute of Technology, Cambridge, MA. In 1997 he joined the MIT Laboratory for Electromagnetic and Electronic Systems as a Postdoctoral Associate, and became a Research Scientist in the laboratory in 1999. In 2001, he joined the MIT Department of Electrical Engineering and Computer Science, where he is presently Professor and Associate Department Head. His research interests include design, manufacturing, and control techniques for power electronic systems and components, and in their use in a wide range of applications. He also consults in industry, and is co-founder of Eta Devices, a startup company focusing on high-efficiency RF power amplifiers. Dr. Perreault received the Richard M. Bass Outstanding Young Power Electronics Engineer Award, the R. David Middlebrook Achievement Award, the ONR Young Investigator Award, and the SAE Ralph R. Teetor Educational Award, and is co-author of seven IEEE prize papers.

David M. Otten received the B.S. and S.M. degrees from the Massachusetts Institute of Technology, in 1973 and 1974 respectively.

In 1974 he joined the MIT Electric Power Systems Engineering Laboratory (EPSEL) as a staff engineer. Since 1984 he has been a Principal Research Engineer in the renamed Laboratory for Electromagnetic and Electronic System (LEES) at MIT. His research interests include instrumentation, power electronics, and the micromouse robot contest.

Khurram K. Afridi (S'93-M'98) received the B.S. degree in electrical engineering from the California Institute of Technology (Caltech) in 1989 and the S.M. and Ph.D. degrees in electrical engineering and computer science from the Massachusetts Institute of Technology (MIT) in 1992 and 1998, respectively. During summers and between degrees he worked for JPL, Lutron, Philips, and Schlumberger. In 1997, he joined the founding team of Techlogix as Chief Technology Officer and became Chief Operating Officer in 2000. From 2004 to 2008 he also led the development of LUMS School of Science and Engineering (SSE) as Project Director, and was appointed Associate Professor and the Werner-von-Siemens Chair for Power Electronics in 2008. From 2009 to 2014 he was a Visiting Associate Professor in the Department of Electrical Engineering and Computer Science at MIT. Since January 2014 he is an Assistant Professor in the Department of Electrical, Computer and Energy Engineering at the University of Colorado (CU) Boulder. His research interests are in power electronics and energy systems incorporating power electronic controls. Dr. Afridi is a recipient of Caltech's Carnation Merit Award, CU Boulder's College of Engineering and Applied Science Dean's Professional Progress Award, and the BMW Scientific Award.